Obviously, this is an oversimplification, since it would imply all collapses *would cease due to pressure support* if they evolve into an adiabatic phase.

The physical resolution of this paradox is that the heating during collapse is curtailed when the gas becomes dense enough to become radiative, so that the effective γ approaches $4/3$, pressure is relieved and *the Jeans mass again becomes independent of density.*

Plot: Jeans Mass Evolution during Free-Fall

• Essentially the fragmented mass corresponds to the minimum mass at the point when the collapse *transitions from isothermal to adiabatically radiative* character, bypassing an adiabatic, but non-radiative phase that would halt collapse. We can estimate this minimum mass as follows.

• The energy liberated in the collapse is clearly $\Delta E \approx 3GM_{\rm J}^2/(10R_{\rm J})$. Averaging this over the collapse time $t_{\rm ff} = \sqrt{3\pi/(32\,G\rho_{\rm J})} \propto R_{\rm J}^{3/2}/M_{\rm J}^{1/2}$ gives a gravitational luminosity (which could be tapped by radiative processes) of

$$L_{\rm ff} \sim \frac{\Delta E}{t_{\rm ff}} \sim \frac{GM_{\rm J}^2}{R_{\rm J}} \frac{(GM_{\rm J})^{1/2}}{R_{\rm J}^{3/2}} = G^{3/2}\left(\frac{M_{\rm J}}{R_{\rm J}}\right)^{5/2} . \qquad (12)$$

This can be set equal to a radiative luminosity of $4\pi R_{\rm J}^2\sigma T^4$ times a radiative efficiency factor ϵ, signalling the epoch when adiabatic evolution starts, i.e. the minimum mass is achieved.

$$G^{3/2}\left(\frac{M_{\rm J}}{R_{\rm J}}\right)^{5/2} \sim L_{\rm ff} \sim L_{\rm rad} \approx 4\pi\epsilon M_{\rm J}^2\sigma T^4 \left(\frac{M_{\rm J}}{R_{\rm J}}\right)^{-2} . \qquad (13)$$

Eqs. (3) and (4) can effect elimination of $R_{\rm J}$ via $M_{\rm J}/R_{\rm J} = 5kT/(G\mu m_H)$, yielding an estimate to the minimum Jeans mass realized in collapses:

$$M_{\rm J}|_{\rm min} = 0.03\,T^{1/4}\,M_\odot \quad , \qquad (14)$$

for temperatures in Kelvin and $\epsilon = 1$ and $\mu = 1$.

∗ This sets the rough lower bound to the mass scale for **protostar** formation: with $T \sim 10\,{\rm K}$ we get $M_{\rm J}|_{\rm min} \sim 0.05 M_\odot$. *No main sequence stars are observed with lower masses*!

Jeans Mass Evolution during Free-Fall

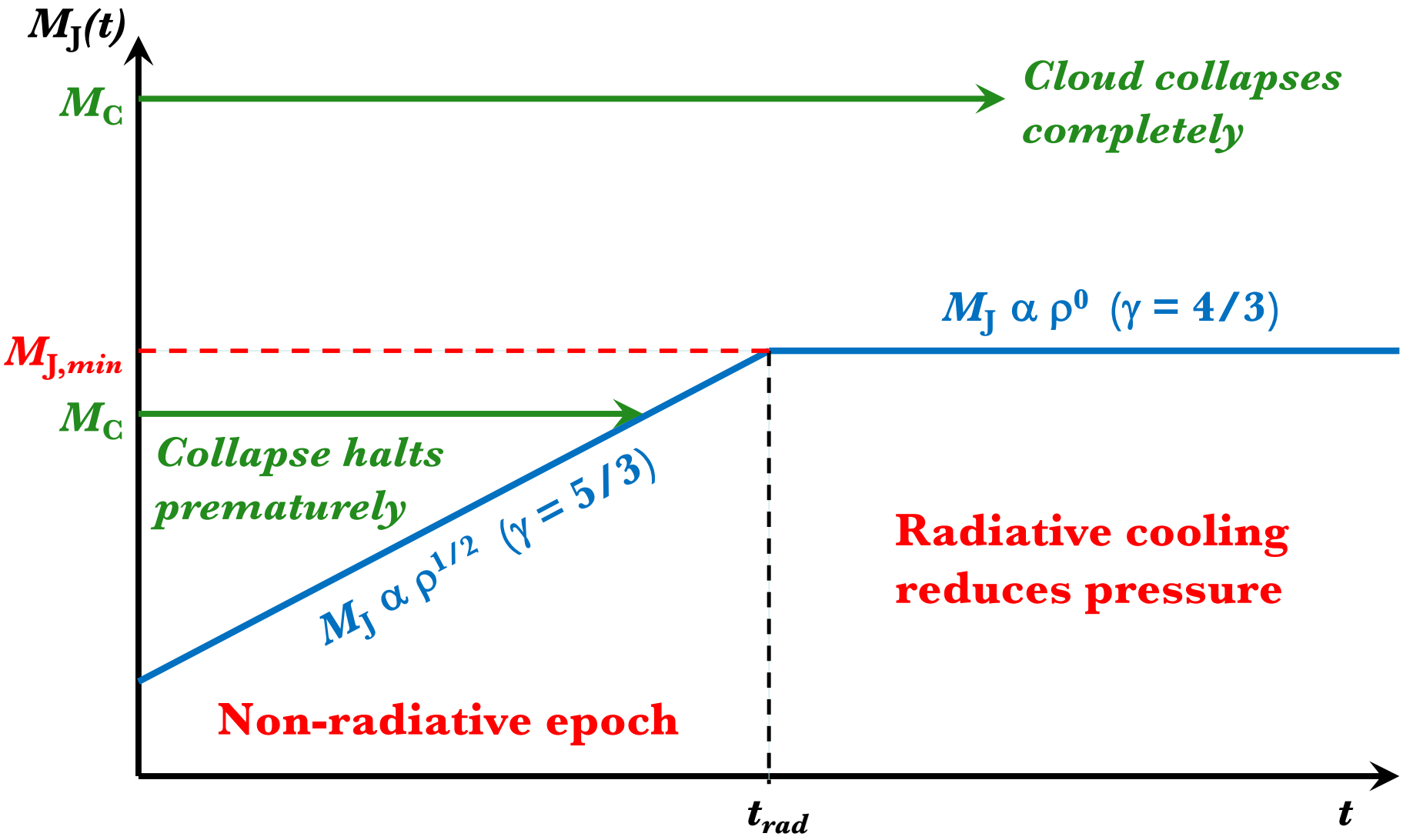

1.2 Pre-Main Sequence Stars

• Collapse starts slowly with a rising temperature and luminosity and then enters a phase where it accelerates at virtually constant luminosity; i.e., $T_e \propto R^{-1/2}$ approximately. Gravitational potential energy seeds the heating. **C & O, Sec. 12.3**

Plot: Cloud Collapse Evolution and Timelines

After $\sim 10^5$ years (i.e. roughly a Kelvin-Helmholtz timescale) for a solar mass protostar, the **Hayashi** track on the H-R diagram is followed, when the effective T is constant, L and R decline promptly. The path of the track is influenced by cloud rotation and magnetic field pressure buoyancy.

Later on, a well-defined and *highly-convective* core develops in this epoch, and again the system enters a constant luminosity phase with increasing temperature and $R \propto T_e^2$. Then the protostar has almost reached the ZAMS.

Plot: Hayashi Pre-Main Sequence Tracks and Timelines

Note: **More massive clouds collapse faster**.

[*Reading Assignment: Hayashi and pre-main sequence tracks, Sec. 12.3*]

• The power spectrum of GMC masses in a turbulent ISM indicates a predominance of lower masses (from lower T regions with smaller $R_{\rm J}$), dictating that most stars form as dwarfs.

Plot: Initial Mass Function (IMF)

• Few stars are massive, generally O and B spectral types. As they are hot, they possess plenty of ionizing UV radiation.

Cloud Collapse Evolution

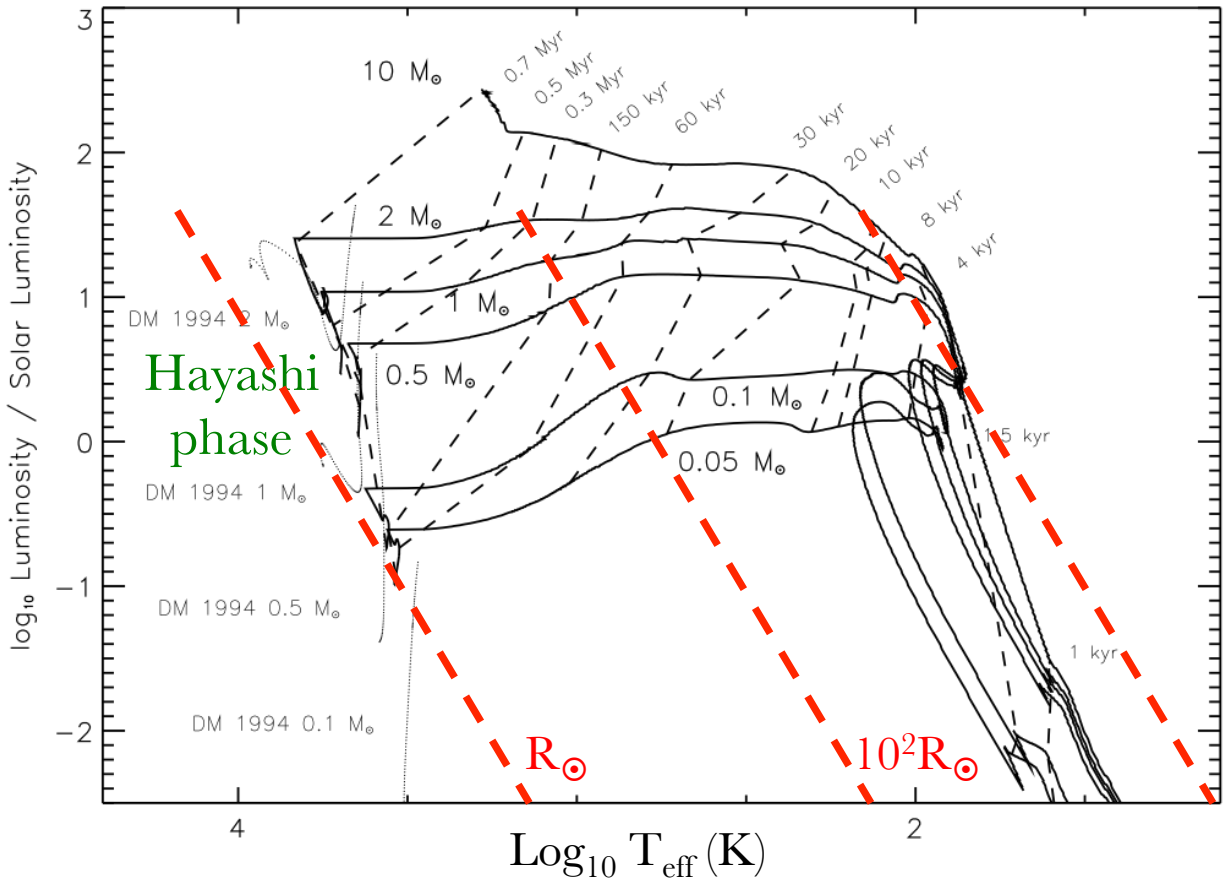

- Pre-Hayashi phase evolutionary tracks in the Hertzsprung-Russell diagram for the collapse and early pre-main sequence evolution of 0.05, 0.1, 0.5,1, 2 and 10 $M_\odot$ cloud fragments (full lines). Dashed lines indicate isochrones for the collapse tracks, labeled with the respective ages. Zero age is defined here as the moment when the respective cloud fragment becomes optically thick and the interior is thermally locked as the first photosphere forms. From Wuchterl & Tscharnuter (A&A **398**, 1081, 2013).

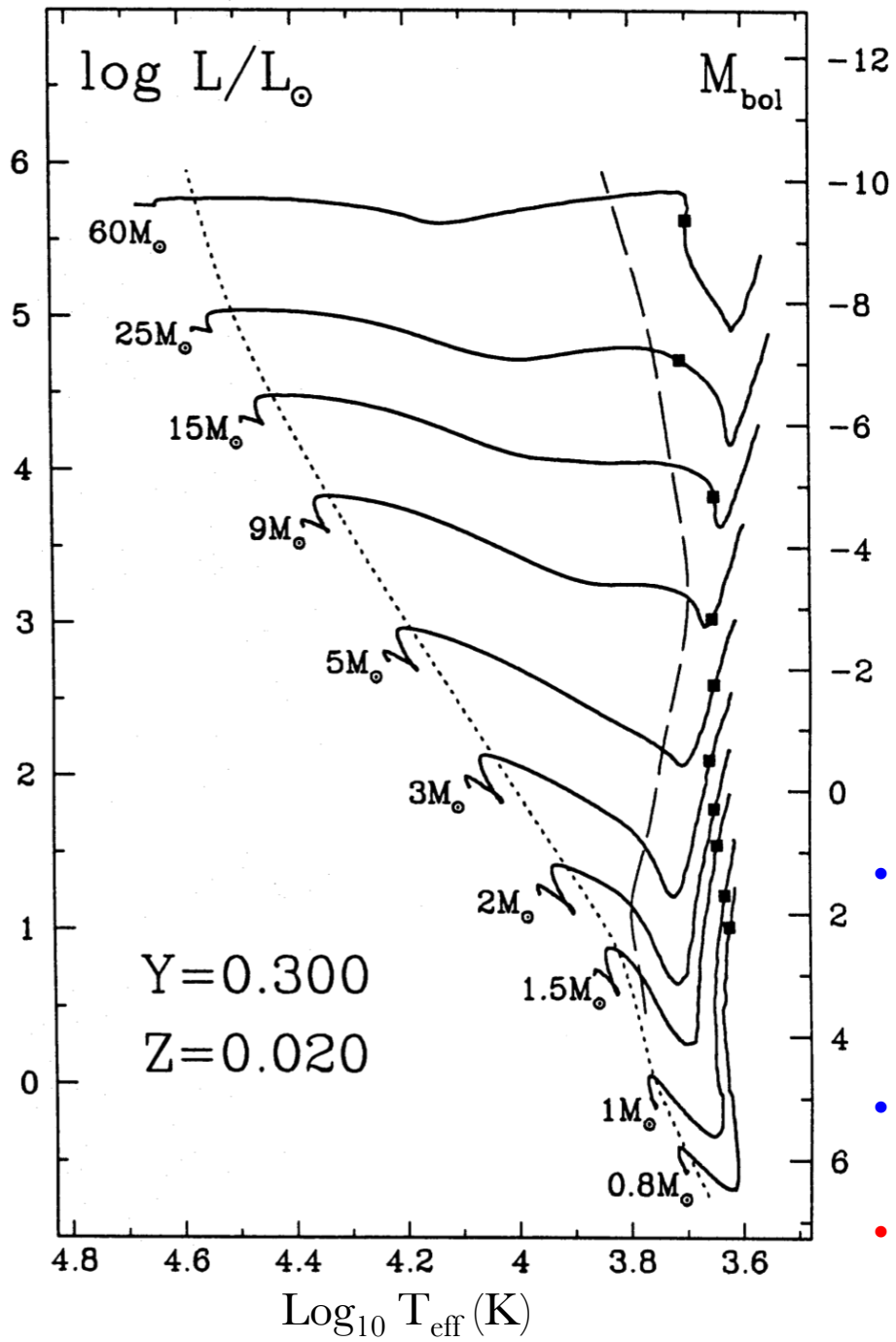

Hayashi Pre-Main Sequence Tracks

Initial mass	Contraction time (Myr)
$60M_\odot$	0.0282
25	0.0708
15	0.117
9	0.288
5	1.15
3	7.24
2	23.4
1.5	35.4
1	38.9
0.8	68.4

- *Left*: Theoretical Hayashi evolution tracks for proto-stars of different masses. Convection is prolific during the horizontal branch "isoluminosity" $T_{eff} \sim R^{-1/2}$ condensing phase.
- *Right*: Table of contraction times (in Myr) for different mass stars.
- Bernasconi & Maeder (A&A **307**, 829, 1996).

Stellar Initial Mass Function

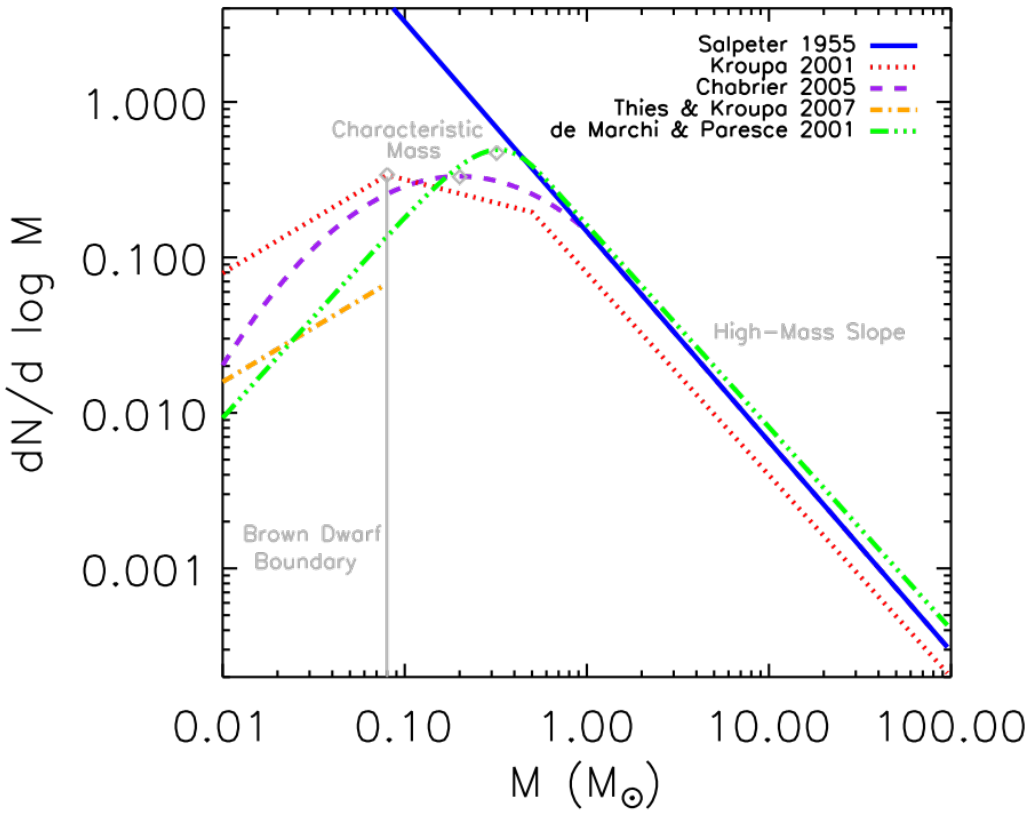

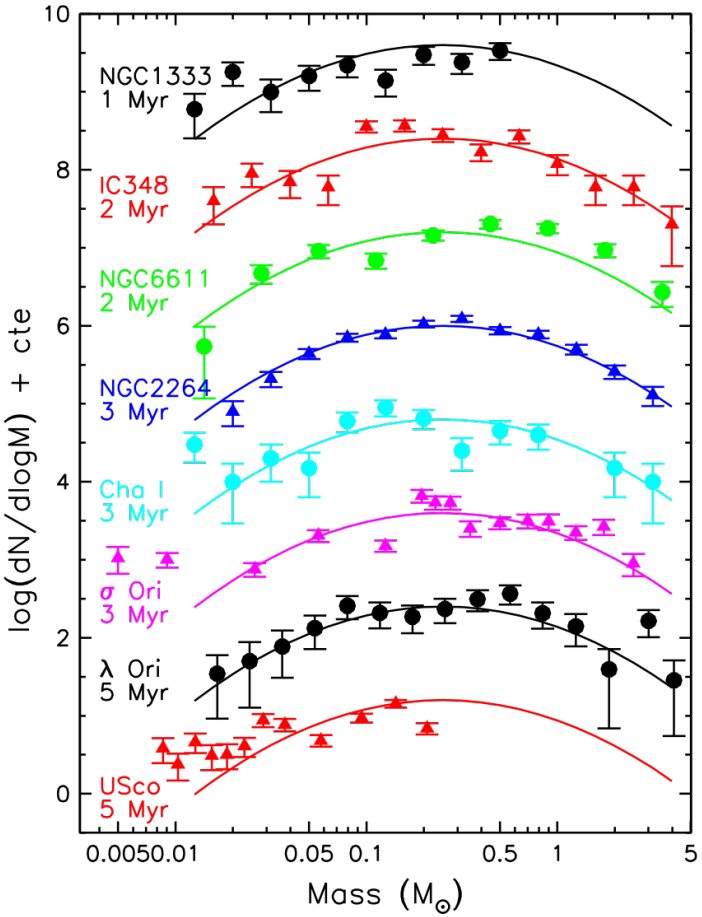

- *Left*: Model IMFs including the original power-law one due to Salpeter (1955). Others address the turn down near the brown dwarf boundary (BDB), and are normalized to unit area.
- *Right*: observational IMFs near and slightly below the BDB from several star forming regions.
- From S. Offner et al., Protostars and Planets VI (2014, **914**, 53).

• Around O and B stars, circumstellar HII regions exist in a **Strömgren sphere** about massive protostellar environments (*draw schematic*). The radius of this sphere directly couples to the stellar UV flux. The dynamical structure of such an HII region is controlled by the rate of recombination

$$\frac{dn_{\rm recom}}{dt} \;=\; \alpha n_e n_{\rm H} \;=\; \alpha n_{\rm H}^2 \tag{15}$$

in the intense UV bath. Here we have invoked charge neutrality $n_e = n_{\rm H}$, and α is the quantum mechanical recombination rate coefficient.

If dN_{UV}/dt is the rate of generation of UV photons by the central star then the HII sphere oblates until all UV photons are absorbed, defining the **Strömgren radius** $R_{\rm S}$, outside of which there exists an HI region:

$$\alpha n_{\rm H}^2 \left(\frac{4\pi}{3}\, R_{\rm S}^3 \right) \;=\; \frac{dN_{UV}}{dt} \;\equiv\; \frac{L_{UV}}{\langle \varepsilon_{UV} \rangle} \quad , \tag{16}$$

with $\langle \varepsilon_{UV} \rangle \gtrsim 13.6\,{\rm eV}$. This solves as

$$n_{\rm H} \;=\; \left(\frac{3}{4\pi\alpha}\, \frac{L_{UV}}{\langle \varepsilon_{UV} \rangle} \right)^{1/2} R_{\rm S}^{-3/2} \quad . \tag{17}$$

If one can measure $R_{\rm S}$ and the UV luminosity blue-ward of 13.6eV, then it becomes possible to infer $n_{\rm H}$ in Strömgren spheres.

• OB stars and HII regions tend to clump together in what we call **OB associations**, spawned by multiple cores in GMCs

Examples of well-formed pre-main sequence objects are **T-Tauri stars**, low mass protostars with very significant winds and associated mass loss.

• These exhibit evidence of expanding *thickish* winds via emission/absorption line diagnostics that reveal **P Cygni** profiles, which can be used for diagnostics on wind speed and shell column density of $n_{\rm H}$.

Plot: P Cygni Line Profile

• Protostellar objects possess angular momentum and are far from spherical. Often, T-Tauri stars possess jets and accretion disks ($\Rightarrow$ aspherical winds): these are called **Herbig-Haro objects**, first identified by Herbig and Haro.

Plot: Herbig-Haro Object Schematic

P Cygni Line Profile

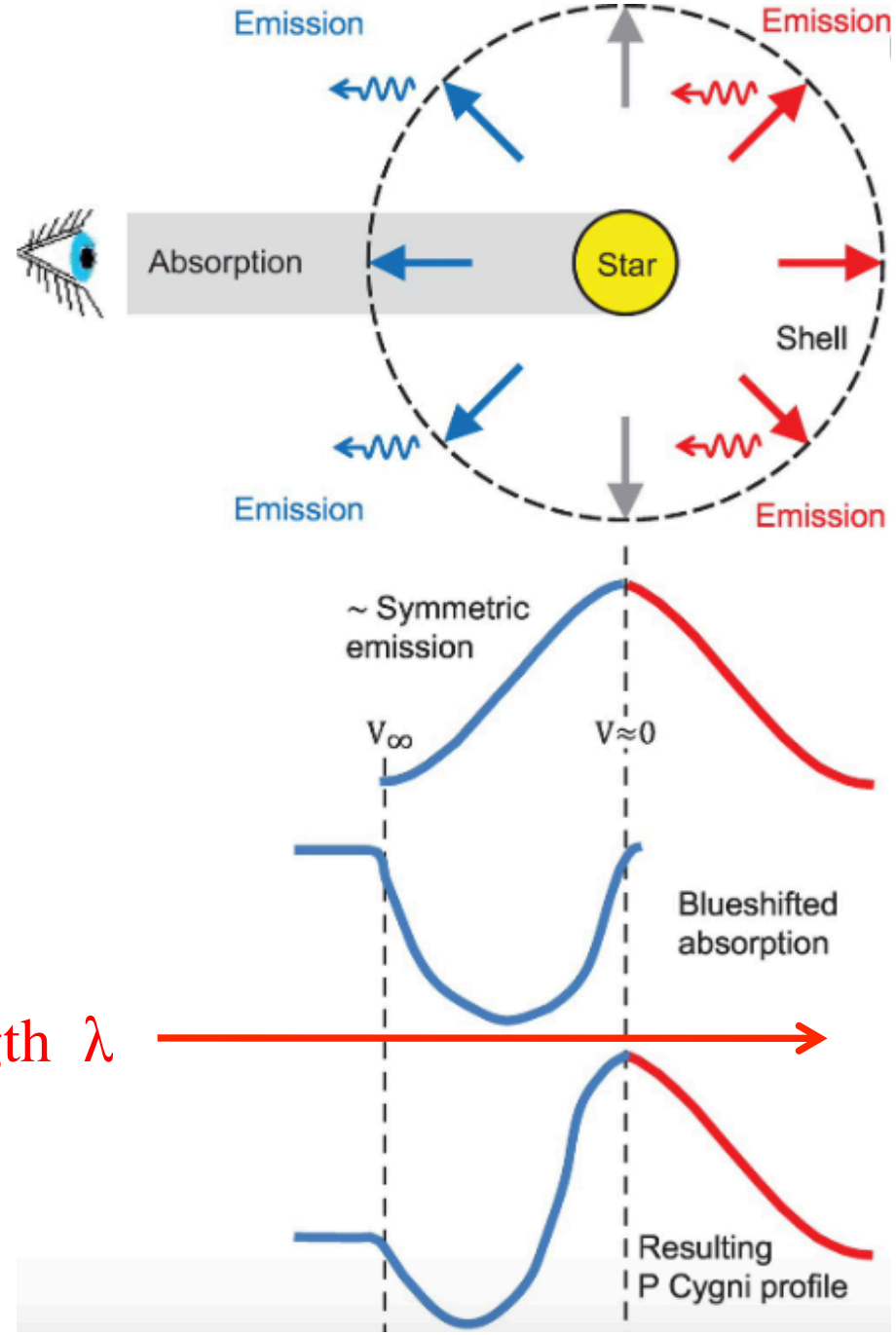

- Credit: R. Walker (LBV Stars, CUP)

Herbig-Haro Object

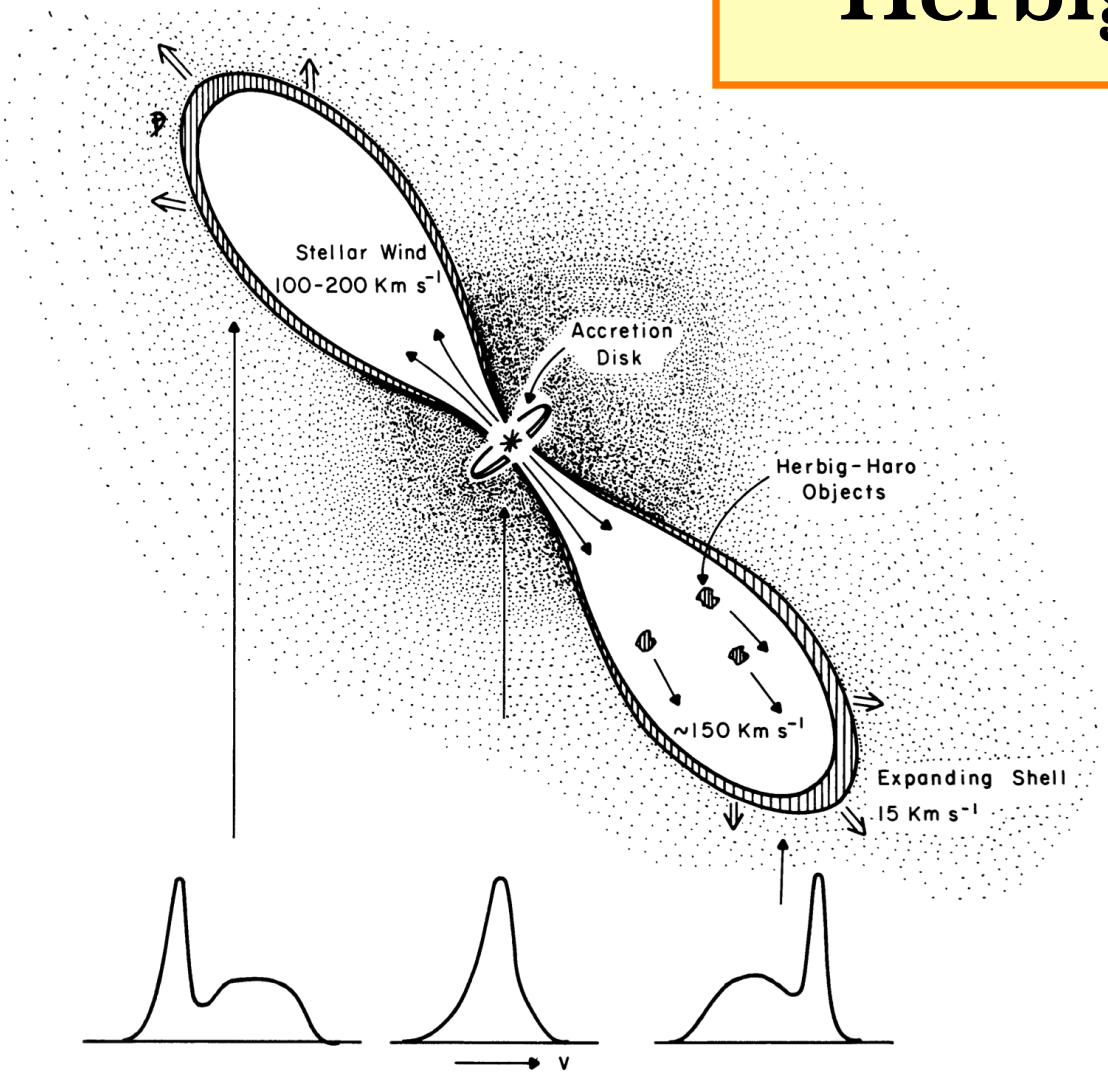

- A model of the T Tauri star in the molecular cloud L1551, with an accretion disk, and a collimated wind/jet named a Herbig-Haro Object.
- Snell, Loren & Plambeck (1980, ApJL 239, L17)

2 Evolution on the Main Sequence

The main sequence in the HR diagram is not a locus of zero thickness due to differing chemical compositions, stages of evolution of the stars, and also due to observational uncertainties. The sun is not quite a **zero age main sequence** (ZAMS) star, having evolved somewhat since birth. **C & O, Sec. 13.2**

• During this evolution, core hydrogen burning in the sun increases the mean molecular weight μ somewhat, reducing the pressure supporting gravity.

∗ The core radius R_c is reduced, $P_c \sim GM_c^2/R_c^4$ rises so that the core temperature T_c rises.

• This pushes the nucleosynthetic luminosity higher, though the energy supply is tapped to expand the stellar envelope to larger radii, in order to satisfy the virial theorem. Eventually, the inflation dominates the use of increased energy generation so that the star only maintains luminosity $\propto R^2 T_{\rm eff}^4$ while dropping its effective temperature $T_{\rm eff}$.

∗ For more massive stars, the increase in radius is more profound, and arises on shorter timescales due to the much more rapid nuclear burning.

∗ This portion of redward evolution on the HR diagram is called the **subgiant branch**. Its endpoint marks when the mass of the helium core is so great that it cannot support the material above it, leading to the giant phase.

Plot: Stellar Evolutionary Tracks on the HR Diagram

• For later stages of the evolution of a solar mass star, once core hydrogen is significantly depleted, the inner structure is a dense helium core with *a surrounding hydrogen-burning shell*. The shell actually burns at *a higher temperature* than the original hydrogen core, due to the new hydrostatic equilibrium involving an isothermal helium core.

Plot: Gaia Hertzsprung-Russell Diagram for Open Clusters

Main Sequence Stellar Evolution

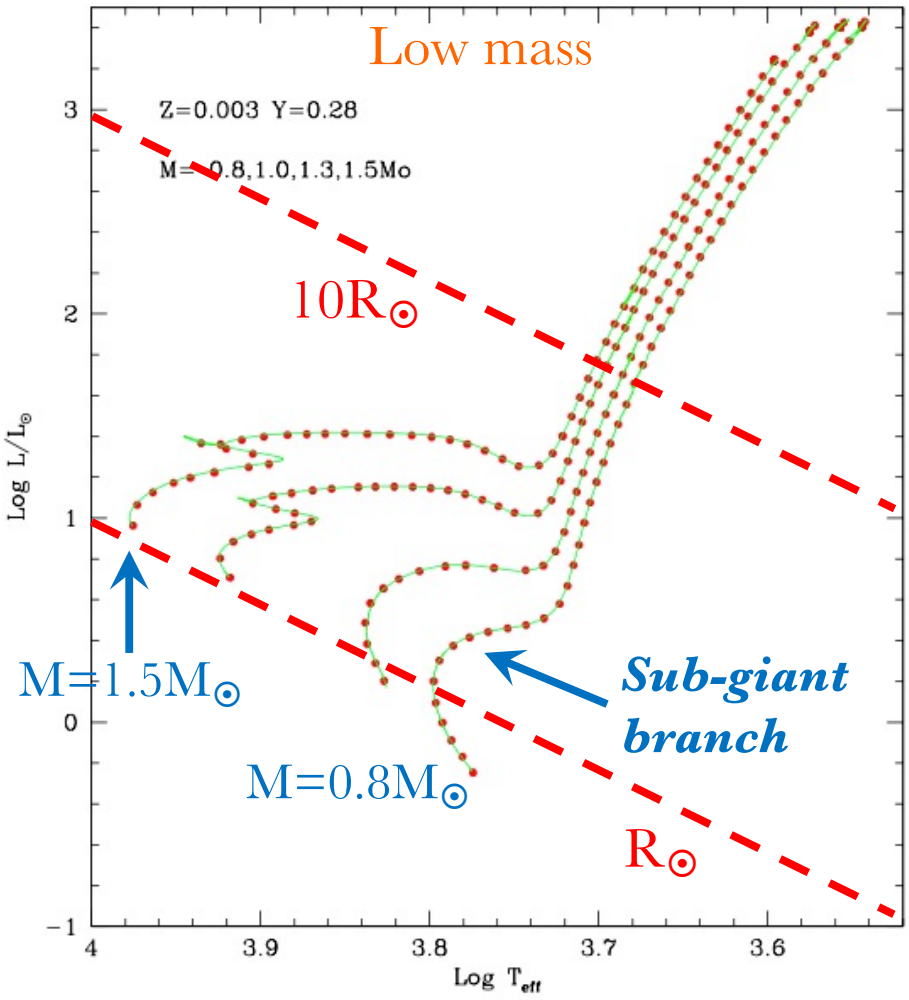

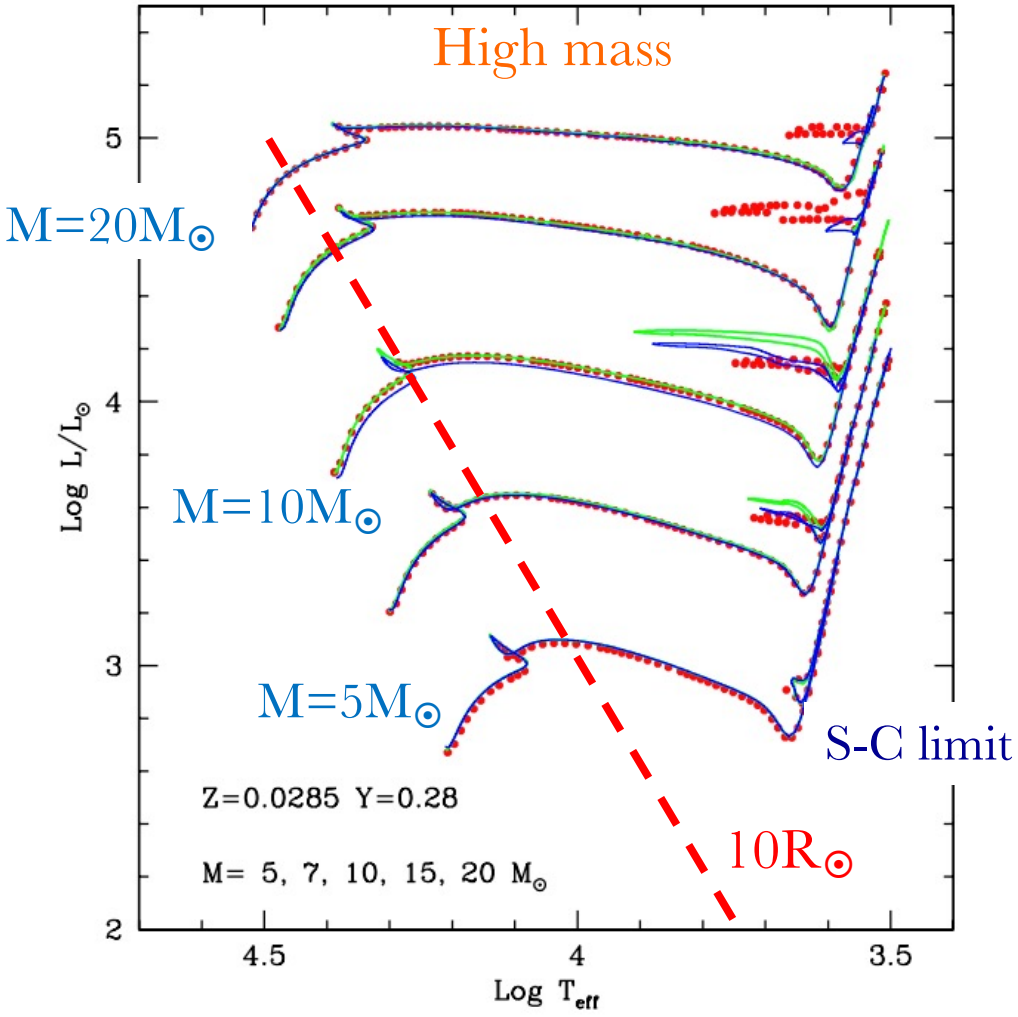

- *Left*: low mass stars. *Right*: high mass stars. Z=metallicity, Y = He mass fraction.
- From G. Bertelli et al., A&A (2008, **484**, 815; 2009, **508**, 355).

Gaia HR Diagram for Open Clusters

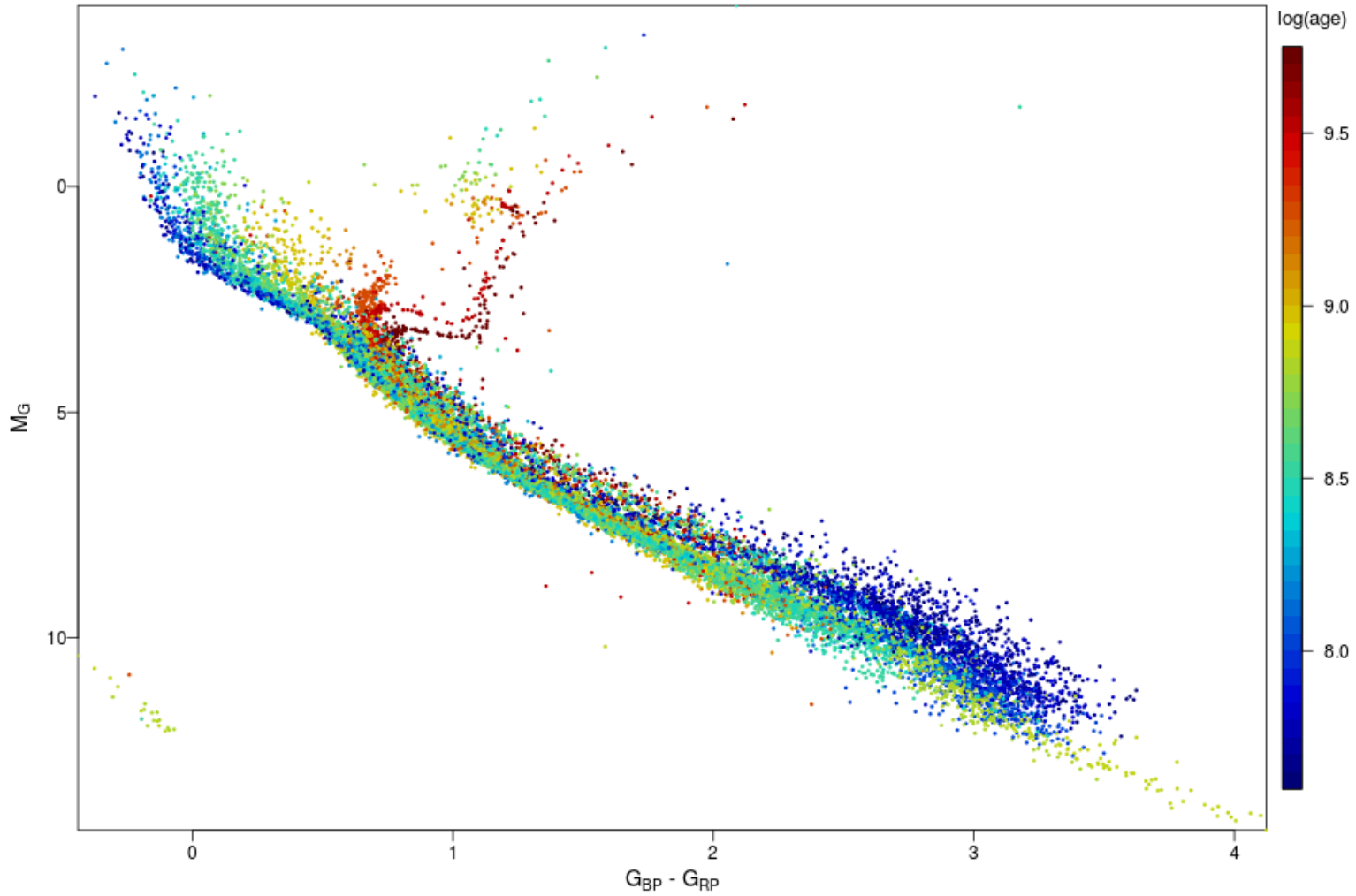

- Observational HR diagram from Gaia Data Release 2 (DR2) for 32 open clusters of main sequence and white dwarf stars. Cluster age is color-coded in years (log scale) according to bar on right. Babusiaux et al. A&A **616**, A10 (2018).